JAST, Vol. 6, No. 1, pp 1–12

JAST
Journal of Aerospace Science and Technology

Analysis of Radial Baffle Effects on Acoustic Characteristics of a Combustion Chamber

Habib ollah Mehrjou[1], Mohammad Farshchi[2], Hadi Mehrjou[3]

An efficient finite volume approach has been used to develop a three dimensional Helmholtz acoustic solver for complex geometries. This acoustic solver was utilized to obtain characteristic mode shapes and frequencies of a baffled combustion chamber. An experimental setup, including stationary and moving sensors, has also been used to measure these quantities for the same model of combustion chamber. Although each of these methods has certain limitations, combination of the numerical results and the experimental data provide the capability to identify complicated acoustical fields created by the combustor complex geometry. Using this approach, the effects of the nozzle convergent section and the number of radial baffles on the chamber's dominant acoustic modes were investigated. It is shown that acoustic solver is capable of capturing major effects caused by the presence of radial baffles and combustor nozzle geometry; however, radial baffles may produce nonlinear effects that cannot be captured by a Helmholtz acoustic solver.

INTRODUCTION

The occurrence of high frequency combustion instabilities in a combustion chamber is associated with the resonant coupling of the chemical heat release process and the chamber acoustic fluctuations leading to growth of the hot gas pressure oscillations in one or more acoustic wave modes within the chamber [1, 2]. Several passive instability control devices have been used successfully to circumvent this problem [3]. Application of radial baffles at the injector face substantially modifies the acoustic resonance properties and changes the oscillatory flow pattern in the vicinity of the injector plate of liquid propellant combustors. Radial baffles are mostly effective with transverse wave motion modification, and are expected to influence pure and mixed tangential modes [3]. Vortices formed at the edge of a baffle blade can also dissipate acoustic energy and increase damping [4]. However the viscous effects are speculated to play a secondary role, and it is the modification of the chamber acoustic mode shapes, especially the transverse modes, that results in cancellation of the resonating mode. This statement is supported by the observation that the existence of radial baffles has a negligible effect on the damping of the longitudinal instability modes [3, 5]. Early studies of the effects of injector face baffles on the stability performance of a combustion chamber were limited to cold acoustic experiments. Wieber [5] examined the acoustic behavior of a cold cylindrical chamber with no mean flow under the influence of various baffle patterns. Wieber observed that radial baffles distorted the acoustic fields by obstructing particle motion in the tangential direction, and hence damped the transverse modes much more effectively than the longitudinal modes. Hence he concluded that the orientation of the baffles with respect to the ordered acoustic field is important. More recently Laudien *et.al.* [6] conducted cold acoustic tests and hot firing tests. They reported that a two-bladed baffle configuration could, at most, prevent tangential modes from spinning. A three-bladed baffle design damps the first and second tangential modes. A four-bladed configuration has no effect on the second tangential mode because it can still develop within the baffle arrangement. The five-bladed design is expected to influence all tangential modes up to the forth. This arrangement shifts the resonant frequency to lower values, especially for the first and

1. *Ph.D., Islamic Azad Univ., Islamshahr Branch, Tehran, Iran.*
2. *Professor, Dept. of Aerospace. Eng., Sharif Univ. of Tech., Tehran, Iran, Email: farshchi@sharif.edu.*
3. *GD of A/C Design, Construction & Certification Office, Tehran, Iran.*

second tangential modes, and increases damping over unbaffled configuration by a factor of five for the first two modes; however, it does not affect the third and the fourth tangential modes. Laudien *et.al.* concluded that based on their own results and those reported by Harrje and Reardon [3], the reasonably good agreement between acoustic cold and hot firing decay rates justifies the use of the acoustic cold chamber models as reasonably accurate approximation of combustion acoustics.

Acoustic mode shapes and frequencies can be obtained by experimental testing of an acoustical model of the chamber or by solution of the three dimensional wave equation for the chamber geometry. Our original intention was to develop an acoustic field solver that could replace any cold experimental testing. The experimental set up was designed to validate the numerical results. However, it was shown that some of the mode shapes predicted by the numerical method are not realized in the experiments, and must be discarded. Nevertheless, the numerical mode shape solutions for the modes that are realized experimentally can be of great assistance in identification and visualization of the mode shape for complex geometries. In the following sections, we shall first describe our experimental setup. A second order accurate finite volume based numerical method and its validation are presented next. Finally numerical results and the experimental data for a sample combustor are presented and discussed in details.

EXPERIMENTAL SETUP

Experiments were designed to determine the characteristic frequencies and the associated three dimensional structures of standing and traveling acoustic waves in a liquid propellant rocket motor combustion chamber. No provisions for gas flow in the model were made. The instrumentation and experimental techniques used in this work were adopted from earlier work relating to determination of acoustic characteristics in full scale rocket motors [5, 6, 7]. However, new experimental techniques were used to map and distinguish the characteristic mode shapes in baffled combustors. These will be discussed in the following.

The internal details of a combustion chamber were used to build a model. A head-end and a nozzle throat closure plates were fabricated. Holes were bored through the sides of the model and through the head-end and the throat closure plates to allow access for acoustic drivers and microphones to the model interior. General geometry of the model and location of access holes are shown in Figure 1. The hole at the center of the throat closure plate was on-axis and permitted a specially designed rod carrying a 1/2 inch microphone to be inserted and moved along the model axis. The rod was equipped with a flip open ninety degrees extension providing for microphone positioning at half an inch apart from radial locations. This microphone carrying rod was connected to a stepper motor creating 360 degrees rotation at an angular speed of five degrees per second. The moving microphone assembly was placed on a rail and moved axially with another stepper motor at the speed of 1.4 millimeter per second, (see Figure 2). Hence, the moving microphone can map the entire combustor volume. The data acquisition system consisted of seven 1/2 inch variable capacitance microphones, pre-amplifiers, variable gain amplifiers, a terminal box, a data acquisition card with eight A/D input channels and four D/A outputs. Data sampling rate was set at 20 KHz per channel. Six of the microphones were fixed at different locations on the combustor sides, and one was moved inside the combustor. The accuracy of a typical microphone was ± 2 dB for the frequency range of 0.1 to 20 kHz and sound pressure level range of 60 to 140 dB. Motion of the moving microphone was automatically controlled by the data acquisition computer system and monitored through two digital cameras. Several speakers were used as acoustic drivers. The sound generation system consisted of a function generator, an amplifier, a digital multimeter, an oscilloscope, and up to three speakers. The maximum speaker amplitude deviation of 4.2 dB from 200 Hz to 5 kHz was measured at the distance of one meter for a one watt input power.

Test procedure consisted of making a "frequency sweep run" using speakers to provide continuous frequency variation. Data from sweep runs contained acoustic amplitude as a function of frequency, resulting in an acoustic spectrogram. This would result in determination of characteristic frequencies of the combustor. To determine the characteristic mode shapes of the chamber, a single frequency sinusoidal signal at a given characteristic frequency is generated by speakers having equal input power. The acoustic pressure field is recorded simultaneously by stationary microphones as well as by the moving microphone while it sweeps the axial and tangential directions at a fixed

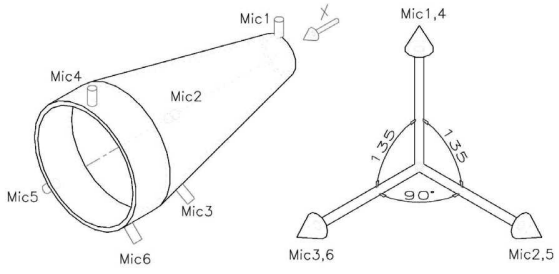

Figure 1. Position of microphone access holes on the combustion chamber.

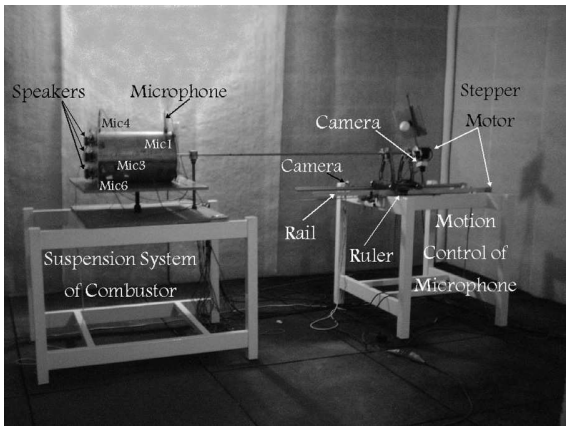

Figure 2. Combustor stand and microphone motion control setup.

radial location. Measurements are then repeated for different radial locations. This provides a complete three dimensional map of the acoustic field inside the chamber. To identify the characteristic mode shape corresponding to a given characteristic frequency, the pattern of nodes and antinodes in the acoustic field is required. The phase angle between the responses from the moving sensor and any of the stationary sensors changes by 180 degrees as the moving sensor crosses a node. Therefore, comparison of a stationary sensor response with that of the moving sensor in addition to the sound pressure level measurements of the moving sensor determines the location of nodes and antinodes of the acoustic field. To the best of our knowledge, the use of this technique has not been reported in the relevant literature before.

GOVERNING EQUATIONS AND NUMERICAL SIMULATION

Finite element based commercial codes such as ANSYS® or NASTRAN® have been used by several investigators to analyze characteristics of acoustic fields inside liquid or solid propellant rocket motors [7, 8]. Lower order pure axial or tangential modes have been of particular interest. In principle, these codes can provide characteristic frequencies and mode shapes for chambers with rather complex geometry. However, it is usually required to implement such an acoustic field prediction code into a stability prediction code. Therefore, researchers have developed their own acoustic field solver [9, 10]. A finite volume approach has been developed by French and Coats [10] for solid propellant rocket motors. They have presented a two dimensional derivation, and have hinted at the three dimensional development.

In the present work, a three dimensional finite volume method for discretization of the Helmholtz equation on a structured or an unstructured grid has been developed. This is a fully implicit method, which results in a matrix whose eigenvalues are directly related to the characteristic frequencies of the chamber. The eigenvector associated with each eigenvalue is also the characteristic acoustic mode shape for the related frequency. This method is then used in a baffled combustor and the effect of baffles in distortion of each mode is identified. The focus of this paper is on higher order pure tangential and mixed transverse modes, which have not been fully treated previously.

Governing Equation

Assuming infinitesimal perturbations in pressure, temperature, velocity and density, Euler equations reduce to the well-known acoustic equation with source terms:

$$\nabla^2 p' - \frac{1}{a^2}\frac{\partial^2 p'}{\partial t^2} = h$$

$$\frac{\partial p'}{\partial n} = -f \qquad (1)$$

where h and f are source terms that originate from mean flow, combustion, nonlinear terms and boundary admittance. Assuming a harmonic wave behavior in time with an angular frequency ω, we have:

$$\nabla^2 p' + k^2 p' = h$$

$$\frac{\partial p'}{\partial n} = -f \qquad (2)$$

where $k = \omega/c$ and c is the speed of sound in the media. Utilizing definition of the acoustic velocity potential and the relation $p' = -\rho_0 \frac{\partial \varphi}{\partial t}$ we can express Eq. (2) in terms of the acoustic velocity potential. Note that the spatial distribution of the acoustic pressure and the velocity potential are identical. The homogeneous form of this equation for the combustion chamber geometry provides the characteristic frequencies and mode shapes of the combustor.

$$\nabla^2 \varphi + k^2 \varphi = 0$$

$$\frac{\partial \varphi}{\partial n} = 0 \qquad (3)$$

This is the well known Helmholtz equation with a Neumann boundary condition. The equation has infinite solutions, each solution being valid for certain k. We use a finite volume discretization method to solve this equation.

Finite Volume Method

We have used a finite volume approach on a three dimensional structured grid. This method is second order accurate with a rather simple boundary condition implementation. To understand the discretization method used here, consider a cubic grid structure with uniform spacing. As depicted in Figure 3, there are 26 grid points around a certain given node (i,j,k) in a three

dimensional grid. Correspondingly, there are 8 cubic volumes around the node (i,j,k) formed by these 26 grid points. Each of the original 8 cubes is subdivided into 8 more cubes. The control volume for integration of the Helmholtz equation is formed by considering 8 of these sub-cubes that surround the (i,j,k) point. This control volume is depicted in the final frame of Figure 3. Next we integrate Eq. 3 over the above control volume:

$$\iiint (\nabla^2\varphi + k^2\varphi)dV = 0 \tag{4}$$

Using the Green's theorem we have:

$$\oiint(\vec{n}.\vec{\nabla}\varphi)dS + k^2 \iiint \varphi dV = 0 \tag{5}$$

φ is considered to be uniform in the above control volume; therefore, the volume integral in Eq. (5) is evaluated easily. To determine the surface integral in Eq. (5), we note that the above control volume is composed of 8 sub-cubes and each sub-cub has three faces shared with other sub-cubs in the control volume and three unshared faces. Since only contributions of the unshared faces count toward the value of the surface integral, then we have 24 faces contributing to the surface integral in Eq. (5). We must evaluate $\vec{\nabla}\varphi$ on each surface. One of these faces is shown in Figure 4. In order to evaluate $\vec{\nabla}\varphi$ on this surface we average it over volume A shown in Figure 4. Therefore, we will

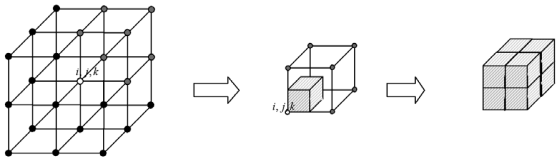

Figure 3. Nodes and volumes around the node (i,j,k) in a 3D grid and the control volume considered.

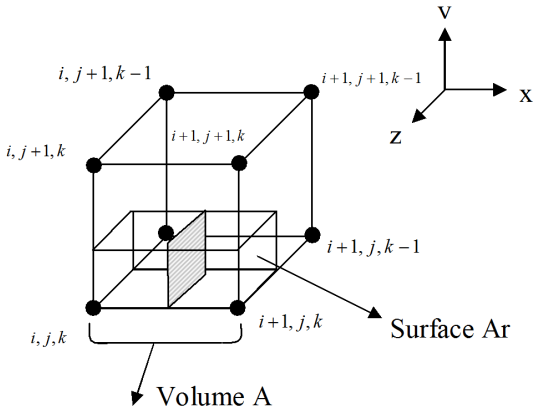

Figure 4. The assigned volume for evaluating $\vec{\nabla}\varphi$ on the dashed surface.

have:

$$\vec{\nabla}\varphi = \frac{1}{V_A}\iiint \vec{\nabla}\varphi\, dV_A \tag{6}$$

Applying the Green's theorem to the above equation we have:

$$\vec{\nabla}\varphi = \frac{1}{V_A}\oiint \vec{n}\,\varphi\, dS_A \tag{7}$$

To perform the above integration, we must have φ and $\vec{n}$ on each surface of volume A. $\vec{n}$ indicates the direction of each surface, and is a unit vector normal to that surface; it is obtained from geometrical considerations. The value of φon each surface is considered as the value of φ at the centre of that surface, and can be evaluated by a simple interpolation. For example φ on the Ar surface (Figure 4) is:

$$\varphi_{Ar} = \frac{1}{16}(9\varphi_{i+1,j,k} + 3\varphi_{i+1,j,k-1} + 3\varphi_{i+1,j+1,k} + \varphi_{i+1,j+1,k-1}) \tag{8}$$

Boundary Conditions

In a rigid-walled axi-symmetric combustion chamber with a closed head-end and closure plates at the throat we have three types of boundary conditions:

- rigid wall boundary condition
- axis boundary condition
- periodic boundary condition

As was mentioned before, the computational control volume shown in Figure 3 consists of 8 cubes that surround the central node (i,j,k). When a node is placed on a rigid wall, then there are four cubes or two cubes that surround that node depending on its location. In this case, rigid wall boundary condition is implemented by just considering the existing cubes and setting the Neumann boundary condition on the faces that are part of the wall. Periodic boundary condition is simply implemented by considering the same condition for nodes that are at $\theta = 0$ and the nodes that are at $\theta = 2\pi$. Axis boundary condition requires special treatment. If the grid is such that there is a rotational symmetry, then the grid lines collide on the axis and cubes change to pyramids. To avoid this problem, we place the first row of nodes at distance $r = 1E-6$ from the axis, and treat it as a rigid wall boundary condition. This way we avoid the axis singularity line, and have hexahedral computational meshes everywhere.

Applying Eq. (5) to every node in the field, and using the above discretization method, we obtain a coupled system of equations for the values of the

velocity potential function at three dimensional mesh points. This is represented in the following form:

$$\bar{\bar{A}}.\vec{\varphi} + k^2\vec{\varphi} = 0 \tag{9}$$

The special form of the system of equations indicates that evaluation of eigenvalues and eigenvectors of matrix $\widehat{A}$ will result in determination of the characteristic frequencies and acoustic mode shapes of the combustion chamber. The generated matrix is non-symmetric and sparse. Due to the large size of the above matrix, iterative methods of eigenvalue determination must be used. These methods find as many eigenvalues as the user demands, and are memory efficient. Lanczos method, Block Lanczos method and Arnoldi method are among the most efficient methods. Lanczos method is used for symmetric matrices, and the other two are used for non-symmetric ones. ARPACK eigensolver package is used here. This free package is based on the Arnoldi method [11]. The output of this package is the eigenvalues and eigenvectors of a sparse matrix. The eigenvectors represent the velocity potential distribution of each mode. Histories of convergence of the first longitudinal and first tangential modes of a cylinder, with both ends closed, are shown in Figure 5.

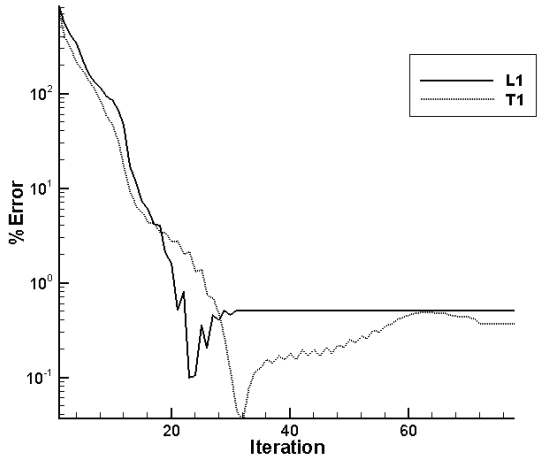

Figure 5. Convergence history of ARPACK.

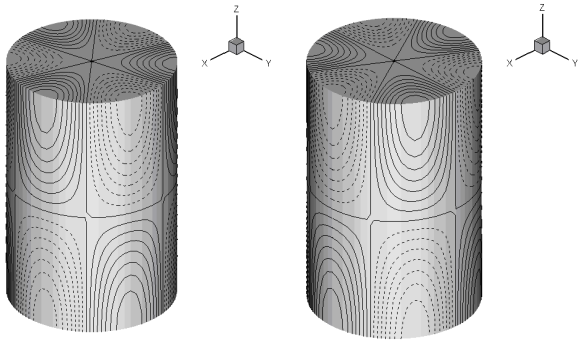

Figure 6. Pressure contours for 3^{rd} tangential-1^{st} longitudinal conjugate modes.

Acoustic Velocity

Acoustic velocity is the gradient of acoustic velocity potential. This gradient is calculated at each node of the domain by averaging it over the control volume around that node:

$$\vec{\nabla}\varphi = \frac{1}{V}\iiint \vec{\nabla}\varphi dV = \frac{1}{V}\oiint (\varphi\vec{n})dS \tag{10}$$

Therefore, in order to compute the acoustic velocity at each node, acoustic velocity potential (φ) and corresponding normal vectors on all outer faces of a control volume must be computed. Since the control volume consists of 8 cubes and each cube has 3 outer faces, then φ should be computed on 24 faces along with the surface area of each face:

$$\vec{\nabla}\varphi = \frac{1}{V}\sum_{i=1}^{24} \varphi_i A_i \bar{n}_i \tag{11}$$

In an axi-symmetric combustion chamber the value of the acoustic velocity assigned to the layer of nodes closest to the axis is set equal to acoustic velocity values at its upper radial level.

Validation

To evaluate the accuracy of the above acoustic solver, the characteristic frequencies and mode shapes of a cylinder with both ends closed are considered. The exact acoustic characteristic of a cylindrical chamber can be obtained analytically [12]. A fine and a coarse grid are generated for this cylinder. The coarse grid consists of 40 nodes in the tangential, θ, direction, 21 nodes in the axial, z, direction and 7 nodes in the radial, r, direction. For the fine grid, these quantities are doubled. Exact and computational results for the first nineteen modes are compared in Table 1. In the mode column, Lx stands for the x^{th} longitudinal mode, Tx stands for the x^{th} tangential mode, and Rx stands for the x^{th} radial mode. Mixed modes are designated accordingly.

Results indicate that the relative error in the finite volume method computations is acceptable even for the coarse grid. The ratio of errors in the two grids for all modes is around 4, which shows that as the grid distance reduces by half, the method becomes 4 times more accurate. This means that the method is fully second order.

The acoustic solver is also capable of capturing conjugate tangential modes, *i.e.*, it provides an orthogonal set of mode shapes for a specific frequency. It is well known that physically there may be two orthogonal mode shapes, called conjugate modes, correspond-

ing to a single tangential mode frequency. In an actual cylindrical combustor, both of these modes have the same probability of existence. If both modes coexist with a 90 degree phase shift, then a spinning mode is formed. Therefore, if a specific characteristic frequency corresponds to two different mode shapes, the acoustic solver is capable of capturing and identifying both mode shapes. Figure 6 shows computational conjugate mode shapes for the third tangential-first longitudinal mode.

RESULTS AND DISCUSSION

We shall first consider effects of several radial baffle configurations on the acoustic characteristics of a cylindrical chamber. Next, we shall examine the effect of the convergent section of the nozzle on the characteristic mode shapes and frequencies of a combustion chamber.

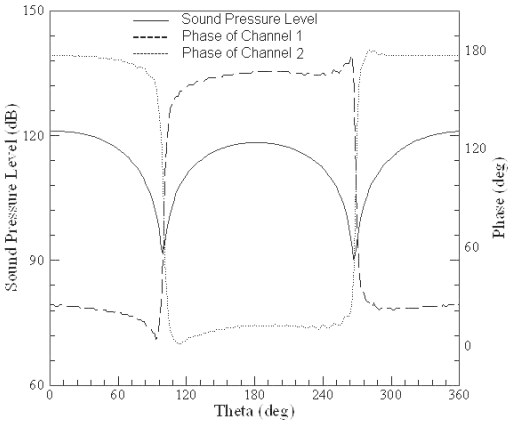

Figure 7. Tangential distribution of sound pressure level and wave phase of the first tangential mode in a cylinder. -Sound pressure level; -Phase of channel 1; -Phase of channel 2.

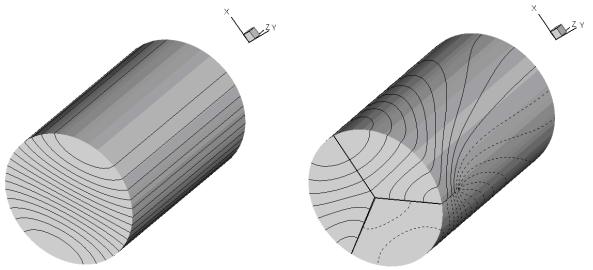

(a) (b)

Figure 8. Longitudinalization of the first tangential mode by radial baffles. a) Unbaffled chamber, b) Baffled chamber.

To study the effects of baffles and geometry changes on the acoustic field of a combustion chamber, two major steps must be taken. First, one should be able to identify a particular characteristic mode shape associated with a given chamber characteristic frequency for the basic chamber geometry without any baffles. This preliminary mode shape recognition is based on the pattern of nodes and antinodes in the acoustic field. Such a pattern can be easily created from the numerical results by plotting the acoustic pressure contours obtained from the acoustic solver. However, in the case of experimental results, we should have a method of identifying the true nodes and antinodes. As we have pointed out previously, the fact that phase angle between the responses from the moving sensor and any of the stationary sensors

Table 1. Exact and computational frequencies for a closed-closed cylinder.

Mode	Exact	Coarse Grid		Fine Grid		Error ratio
		Frequency (Hz)	Error (%)	Frequency (Hz)	Error (%)	
L1	322.4	322.1	0.10	322.4	0.02	4.39
T1	592.0	590.6	0.24	591.7	0.05	4.89
L2	644.9	642.2	0.41	644.2	0.10	4.08
L1T1	674.1	671.2	0.43	673.5	0.10	4.33
L2T1	875.4	867.9	0.86	873.6	0.21	4.10
L3	967.3	958.4	0.92	965.1	0.23	4.02
T2	982.0	974.8	0.73	980.4	0.17	4.40
L1T2	1033.6	1024.1	0.92	1031.4	0.21	4.28
L3T1	1134.1	1117.7	1.44	1130.0	0.36	4.03
R1	1232.5	1215.4	1.39	1228.0	0.37	3.74
L2T2	1174.8	1158.3	1.40	1170.8	0.34	4.13
L1R1	1274.0	1253.9	1.58	1268.7	0.42	3.78
L4	1289.7	1268.6	1.64	1284.4	0.41	4.00
T3	1350.7	1330.0	1.54	1345.8	0.37	4.20
L3T2	1378.4	1349.7	2.08	1371.3	0.51	4.05
L1T3	1388.7	1364.8	1.72	1383.0	0.41	4.17
L2R1	1391.0	1361.9	2.09	1383.5	0.55	3.83
L4T1	1419.1	1388.1	2.19	1411.3	0.55	3.99
L2T3	1496.8	1463.5	2.22	1488.7	0.54	4.10

changes by 180 degrees as the moving sensor crosses a node, is used to map the acoustic field. Therefore, comparison of a stationary sensor response with that of the moving sensor in addition to the sound pressure level measurements of the moving sensor determines the location of nodes and antinodes of an acoustic field. Figure 7 shows the sound pressure level of the first tangential mode of a cylindrical chamber measured by a moving microphone, and its phase change with respect to two of the stationary microphones located at two different tangential positions on a cylindrical combustor. The stationary microphones are positioned at the opposite sides of the first tangential mode nodes.

Figures 8a and 8b show the effect of a three-bladed radial baffle on the first tangential mode of a cylindrical chamber. Figure 8a shows that in an unbaffled chamber, pressure distribution of a pure transverse mode does not vary in the axial direction. However, the presence of radial baffles in a cylindrical chamber changes characteristic frequencies of lateral modes of the chamber, and distorts their mode shapes in the axial direction, as seen in Figure 8b. This effect is known as "longitudinalization" of a transverse mode shape.

The change of the pressure field pattern by the baffles, especially at higher mode numbers, makes it difficult to identify a transverse mode in a baffled chamber with its counterpart in an unbaffled chamber. Therefore, the second step in studying the effects of baffles and geometry changes on the acoustic field is to develop a method to identify a pure transverse mode in a baffled chamber with its counterpart in an unbaffled chamber. Wicker *et.al.* [8] have suggested examining the mode shape pattern in the opposite end of a baffled chamber. This method only works for the first tangential mode, and fails at higher mode numbers. Figure 9 shows the acoustic pressure distributions of the second pure tangential mode at various locations along a three-bladed baffled cylindrical chamber.

Figure 9f indicates that pressure contours at the opposite end of a baffled chamber resemble that of the first pure tangential mode, (see Figure 8a). Therefore, this simple rule may be misleading. Examining results of the numerical acoustic solver for pure transverse and mixed longitudinal-transverse modes of a baffled and unbaffled cylindrical chamber, we concluded that a reliable method is to move up in the frequency scale and examine the mixed mode of the desired transverse mode with the first longitudinal mode. Figure 10 presents acoustic pressure distributions of the mixed second tangential-first longitudinal mode (L1T2) at various cross-sections along the axis of a three-blade baffled cylindrical chamber. Figure 10f shows that the pressure distribution pattern at the opposite end of a baffled chamber is exactly that of the pure second tangential mode shape. Therefore in the characteristic frequency scale, the pure tangential mode just below this mode is the second pure tangential mode. Also, examination of Figure 6 indicates that the combination of the first longitudinal mode with any pure transverse mode in a closed-closed cylindrical chamber creates the pure transverse mode shape at both ends of the cylinder. This allows mode recognition for the case of baffled chambers, where the baffled end distorts the acoustic pressure field, but at the opposite end, the unchanged transverse mode shape is still identifiable.

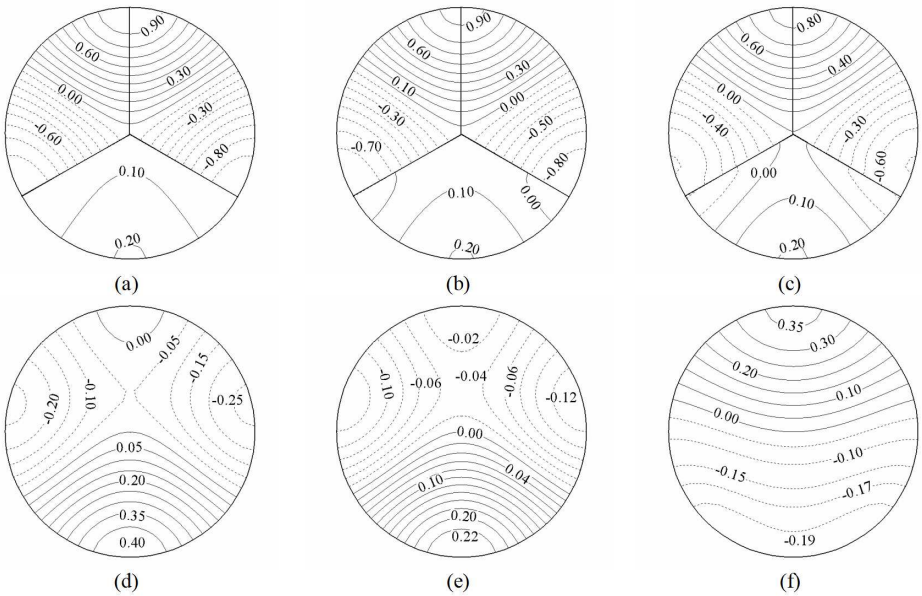

Figure 9. Acoustic pressure distributions of the second tangential mode at various cross-sections, z/L = (a) 0.0, (b) 0.08, (c) 0.14, (d) 0.45, (e) 0.71, (f) 1.00.

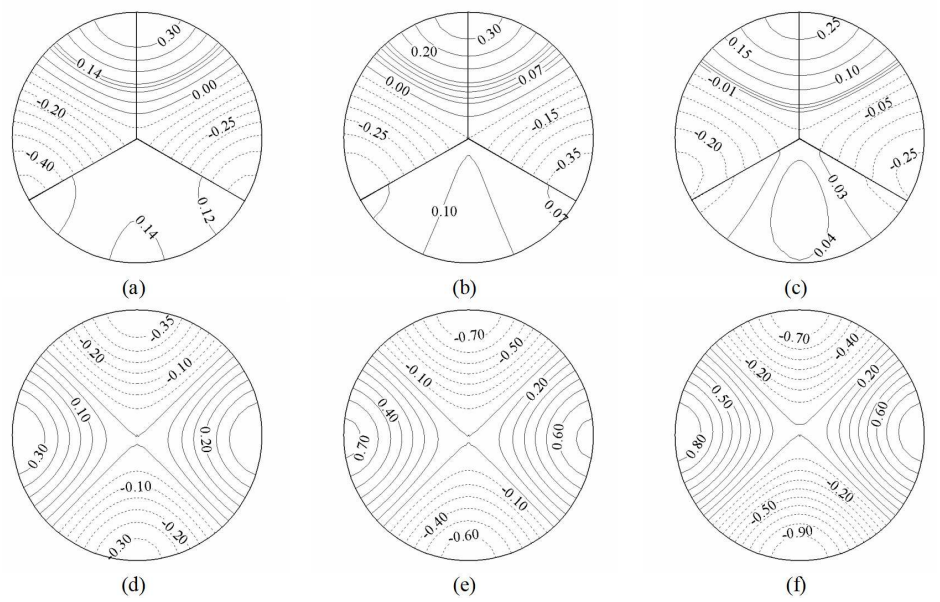

Figure 10. Acoustic pressure distributions of the mixed second tangential-first longitudinal mode at various cross-sections, z/L = (a) 0.0, (b) 0.08, (c) 0.14, (d) 0.45, (e) 0.71, (f) 1.00.

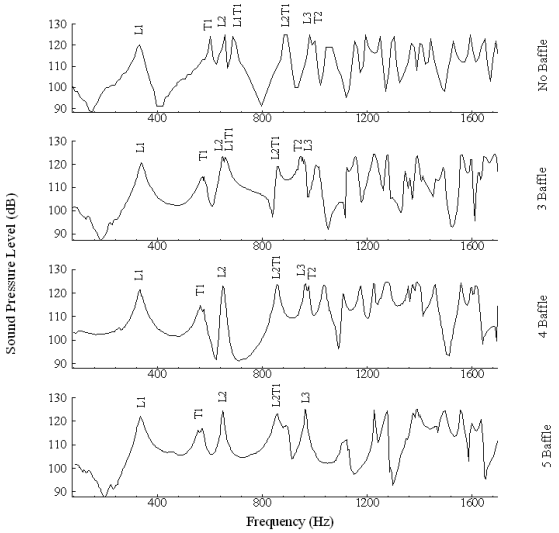

Figure 11. Experimental acoustic spectrum for a cylinder with different radial baffles with L_b/D=0.233.

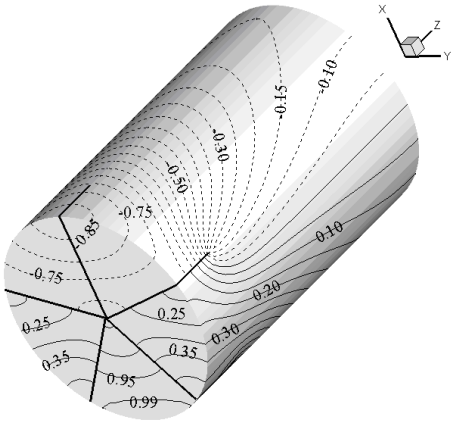

Figure 12. First tangential mode in a cylinder with 5 radial baffles.

Radial Baffle Effects on a Cylindrical Chamber Acoustics

To study the effects of radial baffles on the acoustic field of a cylindrical chamber, we have considered three simple injector face radial baffle configurations. Three, four and five bladed baffles, each blade extending from center of the chamber all the way to its wall, with blade length to chamber diameter ratio (L_b/D) of 0.233 and 0.333 were tested. Figure 11 presents experimentally obtained acoustic spectrums of unbaffled and baffled cylindrical chambers with three, four, and five bladed baffles with L_b/D of 0.233. Table 2 presents numerically and experimentally obtained characteristic frequencies for the above four cases. There are several observations that can be made from these results.

It is expected that radial baffles should have no effect on characteristic frequency of pure longitudinal modes; this is reconfirmed here. Differences in experimentally measured pure longitudinal characteristic frequencies for the above cases are within 2%, and are due to minor test cell climate changes as these tests were conducted over a span of several months.

Reduction of characteristic frequency of tangential modes due to radial baffles has been reported by several researchers [3, 6, 8]. Wicker *et.al.* [8] have considered cylindrical chambers with three, five, and seven bladed baffles, and presented the frequency of

the first pure tangential mode (T1), normalized by that of an unbaffled chamber as a function of the baffle length and the number of blades. Their analysis predicts a 14% frequency reduction for a three-bladed baffle with L_b/D of 0.233, and reduction of 18% for a five-bladed baffle with the same length. Examining numerical results given in the second row of Table 2, we see that our numerical calculations resulted in T1 frequency reduction of 10%, and 13% for the three and five bladed cases, respectively. Present experimental data show even smaller T1 frequency reductions of 5% and 7% for the above cases. Meanwhile, our experiments show that there is almost no reduction of frequency between four and five bladed cases. However, as the baffle length ratio is increased to 0.333, a considerable frequency reduction for the first tangential mode is observed. For a five-bladed baffle with L_b/D of 0.333, our experimental data show a 20% frequency reduction whereas Wicker *et.al.* analysis shows an almost 27% reduction and Laudian *et.al.* [6] reported a 24% reduction.

These results indicate that increasing the number of blades beyond three does not significantly reduce the frequency of the first tangential mode. Closer examination of the numerical solutions indicates that increasing the number of blades in a baffle is effective in localizing the acoustic field and by extension the combustion response to it, whereas increasing the length of blades in a baffle is effective in longitudinalization of tangential modes leading to reduction of their frequency. Figure 12 presents the acoustic pressure distribution for the first pure tangential mode in a cylindrical chamber with a five-bladed baffle. It can be noticed that the magnitude and the spatial gradient of the acoustic pressure at the head-end of the motor is much larger than its counterpart at the other end.

The conjugate spinning modes defined in the previous section are decoupled and do not spin in baffled cylindrical combustor. The baffle blades create a barrier causing slight frequency difference in the conjugate waves, causing them to stop spinning. Examining the results presented in Table 2 for T1 mode, rows 1 and 2, we see that there are slight differences in the numerical results for all baffled cases. The experimentally observed decoupling for the T1 mode is more pronounced than the numerical results. It is seen either as double peaks for T1 mode in the frequency spectrum of a single channel, or as peaks at different frequencies in two different recording channels, (see Figure 13). To see this more clearly, the frequency spectrum of the five-bladed baffled cylinder is magnified near T1 mode using responses from three recording channels and presented in Figure 13. There is an eleven Hertz difference between the two peaks for the T1 mode. Our numerical results indicate that in the case of baffled cylinders, the difference between conjugate frequencies is usually of the order of one Hertz, whereas experimental differences are much larger. This is due to the zero thickness of blades in numerical simulations. The blades are actually modeled as zero normal velocity boundary conditions.

The modification and eventual disappearance of the L1T1 mixed mode in the experimental results can be traced in Figure 11. There are two distinct peaks for L2 and L1T1 in the unbaffled case. These peaks get very close in the case of three-bladed baffle, and the L1T1 mode disappears completely in the case of four and five bladed baffles. It appears that the existence of blades has caused a reduction of the

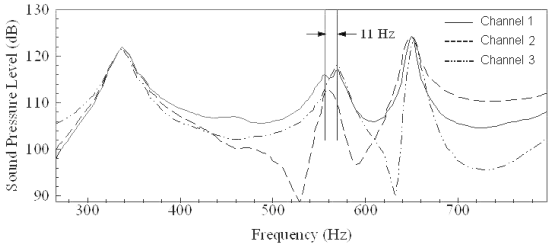

Figure 13. T1 mode conjugate frequencies in a cylinder with 5 radial baffles, Channel 1; Channel 2; Channel 3.

Table 2. Characteristic frequencies in a cylinder with different radial baffles with L_b/D=0.233.

Mode	No Baffle		3 Baffle		4 Baffle		5 Baffle	
	Numeric	Experiment	Numeric	Experiment	Numeric	Experiment	Numeric	Experiment
L1	322.4	334	322.3	341	322.3	331	322.3	337
T1	591.7	603	532.8	573	522.1	564	513.8	560
T1	591.7	603	532.2	577	521.6	577	513.3	571
L2	644.2	657	644.1	646	644.1	655	644.1	652
L1T1	673.5	689	636.5	656	635.7	*	634.9	*
L1T1	673.5	689	636.6	659	635.6	*	634.8	*
L2T1	873.6	894	828.9	849	839.9	853	840.8	859
L2T1	873.6	894	829.5	853	840.0	853	840.9	859
L3	965.1	980	965.0	965	965.0	960	965.0	966
T2	980.4	990	928.1	948	698.8	*	717.4	*
T2	980.4	990	929.0	954	980.3	977	719.9	*

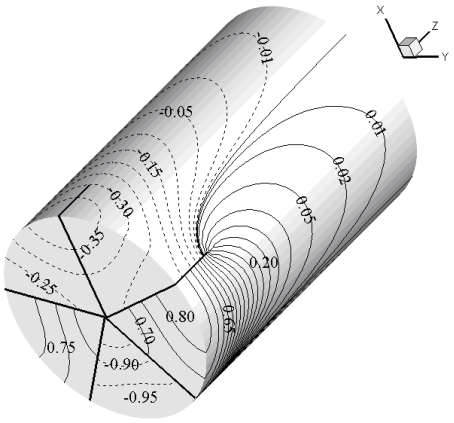

Figure 14. Second tangential mode in a cylinder with 5 radial baffles.

L1T1 characteristic frequency such that this mode has eventually been eliminated in favor of the more energetic second pure longitudinal mode, L2. The numerical solver with its zero thickness baffles and high resolution does predict this trend; however better correspondence with experimental data is expected for finite thickness blades.

Further examination of numerical results and experimental data indicates that there is a major phenomenon that is not captured or is misrepresented by the linear analysis, *i.e.*, the effect of the four and five-bladed baffles on the second pure tangential mode (T2). The four-bladed configuration appears to fix the T2 mode in between its blades, and eliminates one of the conjugates. Experimental data show only one mode at 977 Hz frequency. The numerical method captures two conjugate modes; one with the reduced frequency of 698.8 Hz and the other at 980.3 Hz. There is 281.5 Hz difference between the numerically predicted conjugate modes. Clearly the lower frequency mode is nonphysical and should be discarded. In the case of five-bladed baffle there is no experimental sign of the T2 mode, whereas the numerical results show existence of two conjugate modes at drastically reduced frequencies of 717.4 Hz and 719.9 Hz. Examination of the numerically predicted mode shape for T2 in a five-bladed baffled cylinder (Figure 14) indicates that there is a very large pressure gradient and subsequently acoustic velocities at the tip of the blades, which physically violates the small perturbation assumption of the linear acoustic theory. Therefore, although the linear analysis makes a prediction, it is not physically viable. The existence of such large pressure gradients creates vortical structures that completely damp the second pure tangential mode in a five-bladed baffled cylinder.

Converging Nozzle Effects on a Combustion Chamber Acoustics

A typical liquid rocket engine combustor is composed of a relatively short cylindrical section, and an appropriately sized nozzle converging section. Compared to a cylindrical chamber, the converging nozzle section of a combustor modifies pure longitudinal modes in the radial direction, and pure tangential modes in the longitudinal direction. Numerically obtained acoustic pressure distributions of the first pure tangential and first pure longitudinal modes are shown in Figures 15 and 16, respectively. The word "pure" is a misnomer, and is only used in accordance with nomenclature used for a cylindrical chamber. The converging section of a combustor results in an across the board increase of characteristic frequencies of a combustor relative to a cylinder with the same length and injector plate diameter. Figure 17 presents the acoustic spectrums of a cylinder and an equivalent combustor. Characteristic frequencies of these two cases are given in Table 3.

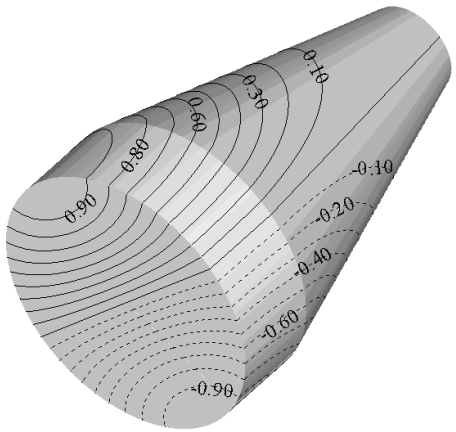

Figure 15. Axial variation of acoustic pressure in 1^{st} tangential mode.

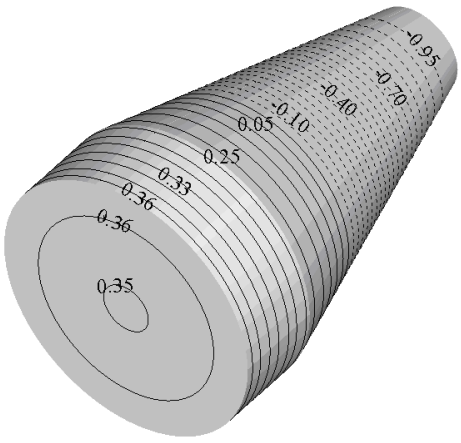

Figure 16. Radial variation of acoustic pressure in 1^{st} longitudinal mode.

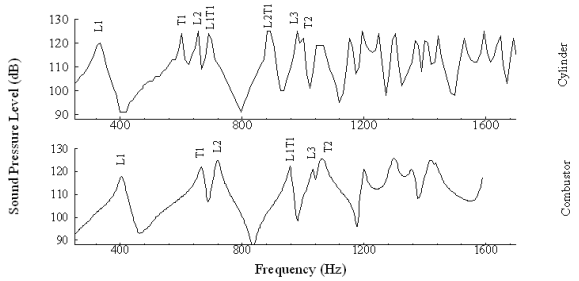

Figure 17. Acoustic spectrum for a cylinder and combustor.

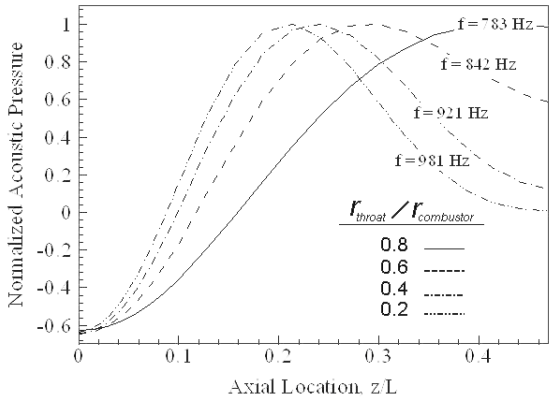

Figure 18. Axial distribution of L1T1 mode acoustic pressure in a combustor for different throat diameters, $r_{throat}/r_{combustor} = 0.8$;

Experimental frequency spectrum (Figure 17) indicates that the L1T1 mode has merged with the L2T1 mode for the combustor geometry considered here. This behavior can be understood by performing a numerical sensitivity analysis of the L1T1 mode shape behavior as a function of the nozzle throat area. Figure 18 presents the axial distribution of the L1T1 mode shape as a function of the nozzle throat area. As the throat area becomes smaller, a pressure node is formed near the throat, making the L1T1 mode shape similar to the L2T1 mode shape. The numerical solver has been able to predict the modification of the L1T1 mode shape due to the nozzle throat changes indicating that any mode shape changes can be captured by the numerical solver as long as the corresponding geometrical changes are included in the model. Recall that in the case of baffled cylindrical chambers, we had zero thickness baffles and the existence of baffles was implemented as a zero velocity boundary condition.

Table 3. Comparison of numerical and experimental frequencies in a cylinder and combustor.

Mode	Cylinder		Combustor	
	Numeric	Experiment	Numeric	Experiment
L1	322.4	334	385.5	405
T1	591.7	603	660.5	668
T1	591.7	603	660.5	668
L2	644.2	657	695.3	722
L1T1	673.5	689	979.6	957
L1T1	673.5	689	979.6	957
L3	965.1	980	1007.9	1034
T2	980.4	990	1055.9	1063
T2	980.4	990	1055.9	1063

CONCLUSIONS

An experimental setup capable of mapping the entire chamber acoustic field and a three dimensional finite volume acoustic solver were developed to study the effects of radial baffles and nozzle geometry changes on the combustion chamber's acoustic field. An experimental technique for mode shape recognition, based on measured acoustic pressure amplitudes and phase changes between the moving and stationary sensors, and a method to identify pure and mixed transverse modes in a baffled chamber have been developed and used in this study. Radial baffles with three, four and five blades, with blade length to chamber diameter ratios (L_b/D) of 0.233 and 0.333 were tested. We have shown that the classical reduction of characteristic frequency of tangential modes due to radial baffles is due to longitudinalization of tangential modes, and is a function of the blade length, and is weakly dependent on the blade numbers. However, increasing the number of blades in a baffle is effective in localizing the acoustic field and by extension, the combustion response to it. Also conjugate spinning modes are decoupled, and do not spin in any baffled combustor independent of the number of blades. On the other hand, the converging nozzle section of a combustion chamber modifies pure longitudinal modes in the radial direction, and pure tangential modes in the longitudinal direction. It also causes an across the board increase of characteristic frequencies of a combustor relative to a cylinder with the same length and injector plate diameter. Existence of some mixed tangential-longitudinal modes in a combustor is dependent on the ratio of the nozzle throat diameter to the combustor head plate diameter. The numerical acoustic solver is capable of capturing all of the above phenomena. However, it cannot completely replace experimental testing. Experimental data indicate that four and five-bladed radial baffles may have nonlinear effects on some of the higher pure and mixed tangential modes that cannot be captured by the linear analysis. Given the inherent shortcomings of a linear analysis; the three dimensional finite volume solver can be a very effective and cost saving tool for geometrical parametric studies in the hands of an informed scientist.

REFERENCES

1. Yang V., Brill T.B. and Ren W.Z., "Solid Propellant Chemistry, Combustion, and Motor Interior Ballis-

tics.", *AIAA Progress in Astronautics and Aeronautics*, **185**, (2000).

2. Yang V. and Anderson W., "Liquid Rocket Engine Combustion Instability", *AIAA Progress in Astronautics and Aeronautics*, **169**, (1995).
3. Harrje D.T. and Reardon F.H., "Liquid Propellant Rocket Combustion Instability", *NASA SP-194*, (1972).
4. Baer M.R. and Mitchell C.E., "Theoretical Evaluation of Rigid Baffles in Suppression of Combustion Instability", *AIAA Journal*, **15(2)**, PP 135-136(1977).
5. Wieber P.R., "Acoustic Decay Coefficients of Simulated Rocket Combustors", *NASA TN D-3425*, (1966).
6. Laudien E., Pongratz R., Pierro R. and Preclik D., "Experimental Procedures Aiding the Design of Acoustic Cavities", *AIAA Progress in Astronautics and Aeronautics*, **169**, PP 377-399(1995).
7. Mathes H.B. and Price E.W., "Methods for Determining Characteristics of Acoustic Waves in Rockets", *AIAA Journal of Spacecraft*, **12(1)**, PP 39-43(1975).
8. Wicker J.M., Yoon M.W. and Yang V., "Linear and Nonlinear Pressure Oscillations in Baffled Combustion Chambers", *Journal of Sound and Vibration*, **184(1)**, PP 141-171(1995).
9. Laverdant A.M., Poinsot T. and Candel S.M., "Mean Temperature Field Effect on the Acoustic Mode Structure in Dump Combustors", *Journal of Propulsion and Power*, **2**, PP 311-316(1986).
10. French J.C. and Coats D., "Automated 3-D Solid Rocket Combustion Stability Analysis", *AIAA paper 99-2797*, (1999).
11. Lehoucq R.B., Sorensen D.C. and Yang C., "ARPACK Users' Guide: Solution of Large Scale Eigenvalue Problems with Implicitly Restarted Arnoldi Methods", *http://www.caam.rice.edu/software/ARPACK*, (1997).
12. Kinsler L.E., Frey A.R., Coppens A.B. and Sanders J.V., *Fundamentals of Acoustics*, John Wiley & Sons Inc., (2000).